ACS Photonics

Article

Cite This: ACS Photonics 2018, 5, 2408−2417

Electroabsorption Studies of Multicolored Lead Halide Perovskite Nanocrystalline Solid Films

Kamlesh Awasthi,[†] Kai-Bo Du,[†] Chi-Yung Wang,[†] Chao-Lin Tsai,[†] Morihiko Hamada,[†] Sudhakar Narra,[†] Eric Wei-Guang Diau,*[,†,‡] and Nobuhiro Ohta*[,†,‡]

[†]Department of Applied Chemistry and Institute of Molecular Science and [‡]Center for Emergent Functional Matter Science, National Chiao Tung University, 1001 Ta-Hsueh Road, Hsinchu 30010, Taiwan

Supporting Information

ABSTRACT: Electroabsorption (E-A) spectra of lead halide perovskites, that is, $CH_3NH_3PbI_{3-x}Br_x$ (x = 0−3), which show large spectral shift depending on the ratio between iodine and bromide, have been measured. By analyzing E-A spectra with the integral method, spectral shape of the absorption spectra for the first exciton band and binding energy of exciton have been determined. Magnitudes of the change in electric dipole moment and molecular polarizability following excitation into the exciton state have been also evaluated in these perovskites. The binding energy of electron and hole in exciton of these materials as well as the magnitude of change in electric dipole moment following exciton absorption is roughly the same, suggesting that the difference of the photoenergy conversion in photovoltaic cells using these materials comes from the difference in light harvesting effect and difference in carrier mobility, not from the difference in carrier generation efficiency. The frequency-dependent third-order nonlinear susceptibility $\chi^{(3)}$ has also been calculated, based on the E-A spectra.

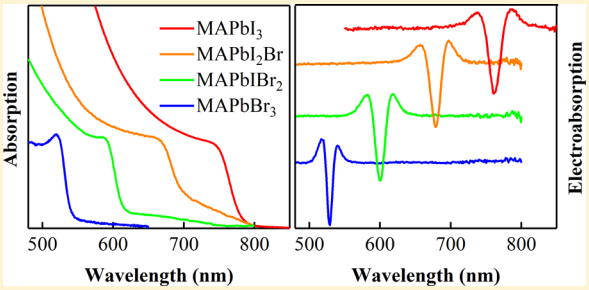

KEYWORDS: *electroabsorption, lead halide perovskite, photovoltaic cell, electric dipole moment, nonlinear susceptibility*

Perovskite structure, that is, a class of crystal with stoichiometry ABX_3 that exhibits so many unique properties, such as superconductivity or ferroelectricity, has received strong attention for a long time.[1−5] Recently, lead halide perovskites have received great attention among photovoltaic community due to their rapid boost in the photoenergy conversion efficiencies of the solar cells fabricated from these absorbers using a very simple low temperature solution processes. For example, photon to electrical power energy conversion of methylammonium lead halide perovskites exceeding 20% has already been reported.[3,6−12] Carrier generation following photoexcitation and carrier mobility in materials as well as in the interface between material and electrode are key issues to determine the performance of photovoltaic cells. Following photoirradition of organic−inorganic lead halide perovskites, coexistence of bound exciton and free charges has been shown.[13,14] It has been also reported that photoconductivity in photovoltaic devices with these materials is attributed to exciton dissociation.[15] To have a high carrier generation, therefore, exciton binding energy should be as small as possible to induce dissociation into free charge carriers by the thermal energy at room temperature, as far as the carrier generation from exciton dissociation is considered. The binding energy of exciton is considered to have strong relation to the electronic structure of materials in the photoexcited state.[16−20] Electric field effects on optical spectra provide information about the change in electric dipole moment following photoexcitation, that is, dipolar properties in the photoexcited state. The charge separated character is expected to be strongly related to the magnitude of the binding energy in the exciton state.[21,22] A large electric dipole moment in the photoexcited state is considered to induce efficient photocarrier generation because of a large distance between hole and electron as well as a small binding energy of hole and electron pair. Based on the electroabsorption (E-A) measurements, therefore, the relation between binding energy of exciton and electric dipole moment in the excited state is expected to be determined.

Photovoltaic parameters of the perovskite solar cells based on a series of $MAPbI_{3-x}Br_x$, where MA is methylammonium and x = 0, 1, 2, and 3, were reported.[23−27] The photocurrent of the devices drastically increases with increasing iodine content in the perovskite film, and absorption extends to the longer wavelength as well. Thus, photon conversion efficiency was reported to agree with the light absorption property of mixed halide perovskites,[23,24] but the difference in photocurrent cannot be explained only by the difference in light harvesting efficiency. In the present study, E-A spectra of bandgap-tunable perovskite thin films of $MAPbI_3$, $MAPbI_2Br$, $MAPbIBr_2$, and $MAPbBr_3$, whose SEM images are shown in Figure 1, have been measured, and the observed E-A spectra have been analyzed with the integral method. In the results, exciton absorption spectra have been clearly determined in every sample, and the

Received: February 9, 2018
Published: May 11, 2018

DOI: 10.1021/acsphotonics.8b00185
ACS Photonics 2018, 5, 2408−2417

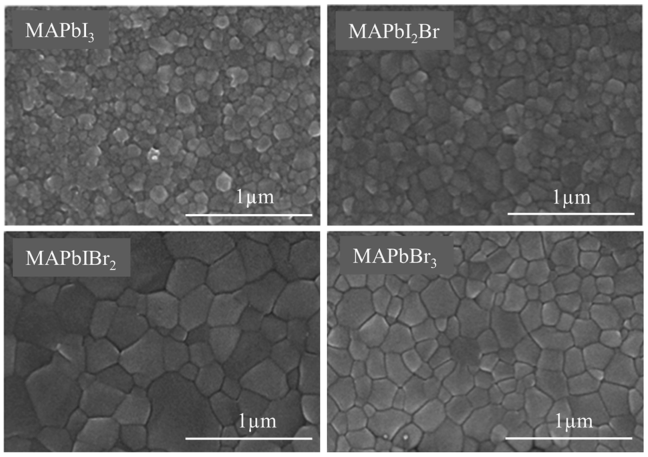

Figure 1. SEM images of $MAPbI_3$, $MAPbI_2Br$, $MAPbIBr_2$, and $MAPbBr_3$ crystals prepared in the present study.

binding energy of exciton of hole and electron pair has been determined. The magnitudes of the change in electric dipole moment and molecular polarizability have been also determined in these samples. Those parameters have been compared with each other and with the ones reported so far in $MAPbI_3$.[28] Based on the results, the origin of the difference of photoenergy conversion efficiency in photovoltaic devices constructed with these materials of $MAPbI_{3-x}Br_x$ has been discussed. Plots of the third-order nonlinear susceptibility of $MAPbI_{3-x}Br_x$ nanocrystalline sample have been also simulated from the E-A spectra and the corresponding absorption spectra.

THEORETICAL BACKGROUND OF E-A SPECTRA

In the presence of electric field ($\mathbf{F}$), molecular energy level is shifted by $-\boldsymbol{\mu}\mathbf{F} - \boldsymbol{\alpha}\mathbf{F}^2/2$, depending on the electric dipole moment ($\boldsymbol{\mu}$) and the molecular polarizability ($\boldsymbol{\alpha}$). As a result, the so-called Stark shift is observed; absorption transition energy is shifted by ΔE ($= -\Delta\boldsymbol{\mu}\mathbf{F} - \Delta\boldsymbol{\alpha}\mathbf{F}^2/2$), where $\Delta\boldsymbol{\mu}$ and $\Delta\boldsymbol{\alpha}$ are the differences in electric dipole moment and molecular polarizability, respectively, between the ground state (g) and excited state (e), that is, $\Delta\boldsymbol{\mu} = \boldsymbol{\mu}_e - \boldsymbol{\mu}_g$ and $\Delta\boldsymbol{\alpha} = \boldsymbol{\alpha}_e - \boldsymbol{\alpha}_g$. The theory shows that the field-induced change in absorption intensity of an isotropic sample at wavenumber ν, that is, $\Delta A(\nu)$, can be given by a sum of the zeroth, first, and second derivatives of the absorption intensity $A(\nu)$ as follows:[29−32]

$$\Delta A(\nu) = (fF)^2\left[A_\chi A(\nu) + B_\chi \nu \frac{\mathrm{d}}{\mathrm{d}\nu}\left(\frac{A(\nu)}{\nu}\right) + C_\chi \nu \frac{\mathrm{d}^2}{\mathrm{d}\nu^2}\left(\frac{A(\nu)}{\nu}\right)\right] \quad (1)$$

Here f is the internal field factor and $F = |\mathbf{F}|$. E-A spectra depend on the angle between the direction of $\mathbf{F}$ and the polarization direction of electric vector of the absorption light, that is, χ. In immobilized and randomly distributed system, the coefficient A_χ depends on the field-induced change in transition moment. With the magic angle χ, that is, 54.7°, B_χ and C_χ are given as follows:

$$B_\chi = \frac{\Delta\bar{\alpha}}{2hc}, \quad C_\chi = \frac{|\Delta\mu|^2}{6h^2c^2} \quad (2)$$

where $\Delta\bar{\alpha}$ denotes the trace of $\Delta\boldsymbol{\alpha}$, that is, $\Delta\bar{\alpha} = (1/3)\mathrm{Tr}(\Delta\boldsymbol{\alpha})$.

In the analysis of the observed E-A spectra using the above equation, that is, so-called differential method, spectral shape of each absorption band should be clearly separated because the magnitudes of $\Delta\boldsymbol{\mu}$ or $\Delta\boldsymbol{\alpha}$ depend on the absorption band. When the separation of the absorption bands is very difficult or when very weak absorption band which shows a large field effect is buried under the strong absorption band, the integral method analysis of the E-A spectra may be very useful, that is, the following integrals of the E-A spectra along the wavenumber are considered:[33,34]

$$\int \Delta A(\nu)\mathrm{d}\nu \cong (fF)^2\left\{A_\chi \int A(\nu)\mathrm{d}\nu + B_\chi A(\nu) + C_\chi \frac{\mathrm{d}A(\nu)}{\mathrm{d}\nu}\right\} \quad (3)$$

$$\int\left\{\int \Delta A(\nu)\mathrm{d}\nu\right\}\mathrm{d}\nu \cong (fF)^2\left[A_\chi \int\left\{\int A(\nu)\mathrm{d}\nu\right\}\mathrm{d}\nu + B_\chi \int A(\nu)\mathrm{d}\nu + C_\chi A(\nu)\right] \quad (4)$$

The first derivative term in the E-A spectra gives a shape of the absorption spectrum in the first integral of the E-A spectra, while the second derivative term in the E-A spectra gives a spectrum whose shape is the same as the one of the first derivative and zeroth derivative, respectively, in the first and second integrals of the E-A spectra. In fact, the absorption spectra of the exciton band of perovskite samples severely overlap with the broad free carrier absorption band, and the field-induced change in absorption intensity seems to occur only for the exciton band. Therefore, the integral method is extremely useful to analyze the E-A spectra of the perovskites, as shown below.

RESULTS AND DISCUSSION

Electroabsorption Spectra. E-A spectra of perovskite samples of $MAPbI_{3-x}Br_x$ (x = 0, 1, 2, and 3) were obtained at the second harmonic of the modulation frequency of the applied electric field with a field strength of 0.3 $MVcm^{-1}$. The results are shown in Figure 2, together with the absorption spectra. Schematic layer structure of FTO/$MAPbI_{3-x}Br_x$/PMMA/Ag used for the E-A measurements and one example of the SEM images with $MAPbI_3$ crystals are shown in Figure 3. Excitation light proceeded perpendicular to the plane surface of the sample, and transmitted light was monitored. Actually, a field-induced change in transmitted light intensity relative to the total intensity of the transmitted light, that is, $\Delta I_{EX}/I_{EX}$ was measured, as will be mentioned in the section of Materials and Method. As shown in Figure 4 for $MAPbI_3$, the field-induced change in absorption intensity is proportional to the square of the applied electric field. The similar field strength dependence was obtained in other samples of $MAPbBr_3$, $MAPbIBr_2$, and $MAPbI_2Br$, as shown in Supporting Information (SI, Figures S1−S3). X-ray diffraction (XRD) patterns of the prepared mixed lead halide perovskite films observed at room temperature in the region of the tetragonal (220) and cubic (200) reflections (2θ = 27−31), which are shown in SI (Figure S4), are essentially the same as the ones shown in the literature.[23] As the iodine content increases, the diffraction peaks in the XRD spectrum shift to smaller angles (Figure S4), whereas absorption spectra shift to longer wavelength as a whole, as shown in Figure 2. In the absorption spectra, the band which corresponds to the bandgap transition, that is, the so-called exciton band overlaps with the broad continuum band, which corresponds to the transition from the valence state to the conduction state, and the separation between these bands is not

DOI: 10.1021/acsphotonics.8b00185
ACS Photonics 2018, 5, 2408−2417

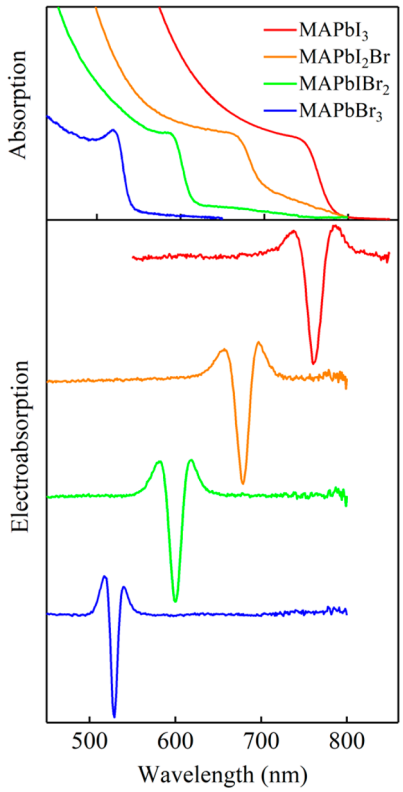

Figure 2. Absorption and E-A spectra of $MAPbI_3$, $MAPbI_2Br$, $MAPbIBr_2$, and $MAPbBr_3$. Applied electric field was 0.3 $MVcm^{-1}$.

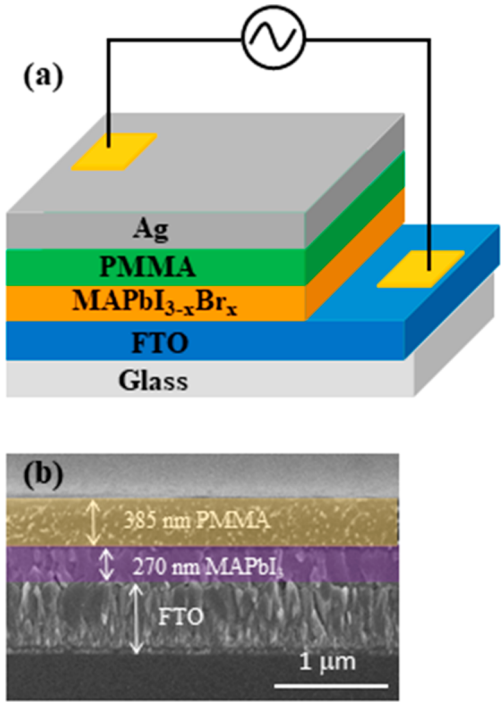

Figure 3. Schematic layer structure of FTO/$MAPbI_{3-x}Br_x$/PMMA/Ag used in the E-A measurements and SEM image of the sample with $MAPbI_3$.

easy, though it is known that the exciton band is located in the longer wavelength region.

When absorption band which shows large Stark effect is buried under strong absorption band(s) or severely overlapped

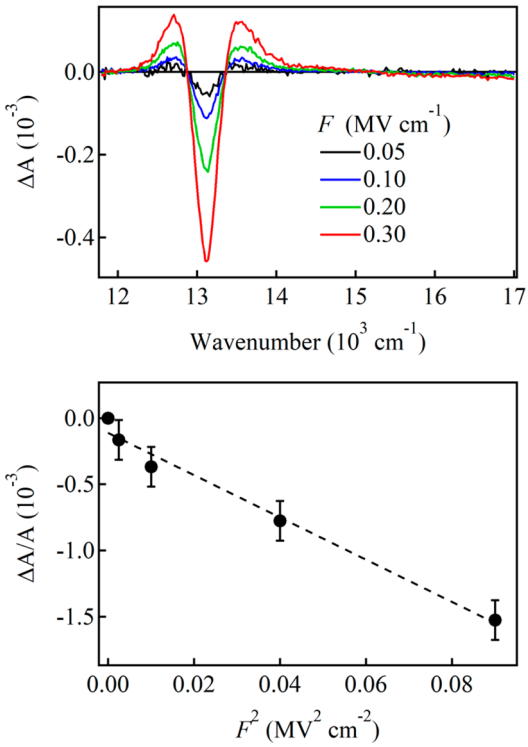

Figure 4. Field strength dependence of the E-A spectra of $MAPbI_3$, and plots of the magnitude of the field-induced change in absorption intensity relative to the absorption intensity as a function of the square of *F*. Plots were obtained at the minimum of the E-A spectra.

with other absorption bands, the so-called integral method is very useful to analyze the E-A spectra.[33,34] In the case of $MAPbI_{3-x}Br_x$, it is likely that the exciton absorption band severely overlaps with a continuum absorption band, as shown in Figure 2. Then, the first integral and the second integral of the observed E-A spectra were taken. The results of $MAPbI_3$ are shown in Figure 5. As mentioned already, the second integral of the E-A spectrum that gives the second derivative of the absorption spectrum in shape should show the spectrum whose shape is the same as the absorption spectrum. When the second integral of the E-A spectrum is watched from this point of view, one peak that corresponds to the exciton band is clearly seen in Figure 5, indicating that the E-A spectrum of the exciton band is mainly given by the second derivative of the absorption spectrum. The absence of other peak in the second integral spectrum indicates that it is not necessary to consider other absorption bands which give the second derivative of the absorption spectrum. The fact that E-A signal at wavenumbers higher than 14500 cm^{-1} is negligible indicates that the E-A signal of the continuum band is negligible.

When the electric field effect is considered in semiconductors, the applied field may result in the Franz-Keldysh effect caused by the field-induced modification of the band structure.[35] In such a case, the Franz-Keldysh oscillation may be expected to be observed also in the continuum band. In the present E-A absorption spectra of all the perovskite samples, however, it is likely that the field-induced change in absorption intensity results only from the exciton band. The first and second derivative components in the E-A spectra correspond to the spectral shift and spectral broadening induced by application of electric field in exciton band. The intensity of the first integral of the E-A spectrum at large wavenumbers

DOI: 10.1021/acsphotonics.8b00185
ACS Photonics 2018, 5, 2408−2417

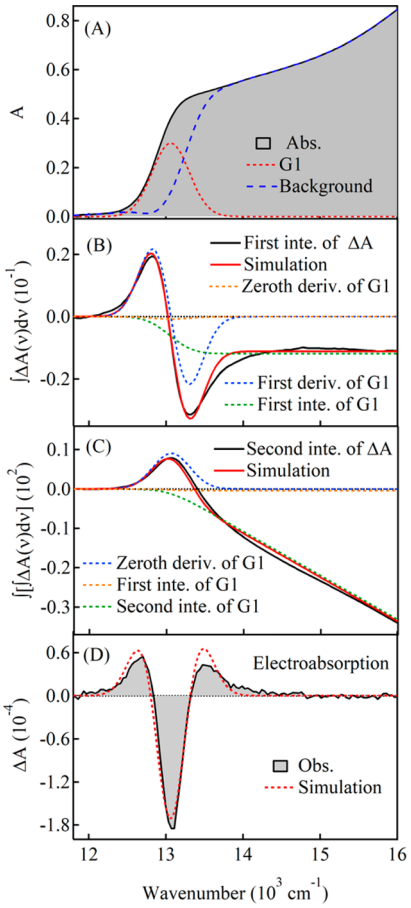

Figure 5. Integral method analysis of the E-A spectra of $MAPbI_3$. From top to bottom, absorption spectrum, the first integral of the E-A spectrum, the second integral of the E-A spectrum, and E-A and simulated spectra.

around 16,000 cm^{-1} is not zero, which results from the contribution of the zeroth derivative component of the exciton absorption spectrum in the E-A spectra. The results that the second integral monotonically decreases with increasing excitation wavenumber also agree with the one expected from the second integral of the absorption spectrum, which may have a Gaussian shape.

As shown in eq 3, the first integral of the E-A spectrum should be given by a linear combination of the zeroth and first derivatives and the first integral of the exciton absorption spectrum. The second integral of the E-A spectrum should be given by zeroth, first, and second integral spectra of the exciton absorption band. Under this consideration, the exciton absorption band superimposed with the continuum band was simulated by assuming that the absorption shape is symmetrical. In fact, the observed E-A spectrum and its first and second integral spectra could be reproduced well by employing the simulated exciton absorption spectrum, its first and second derivative spectra, and its first and second integral spectra, as shown in Figure 5. Based on the above-mentioned integral method analysis, the coefficients A_χ, B_χ, and C_χ in eqs 1, 3, and 4 were obtained, and the magnitude of $\Delta\mu$ and $\Delta\bar{\alpha}$ were determined with eq 2. The results are shown in Table 1. The peak position and bandwidth of the exciton band simulated using the integral method are also shown in Table 1.

E-A spectra of $MAPbI_2Br$, $MAPbIBr_2$, and $MAPbBr_3$ have been similarly analyzed using the integral method, as shown in

Table 1. Evaluated Physical Parameters, that is, the Difference in Polarizability ($\Delta\bar{\alpha}$) and Electric Dipole Moment ($\Delta\mu$), the Peak Position and Bandwidth of the Exciton Band of $MAPbI_3$, $MAPbI_2Br$, $MAPbIBr_2$, and $MAPbBr_3$ Obtained with the Integral Method Analysis of the E-A Spectra

	$\Delta\bar{\alpha}$ (Å^3)	$\Delta\mu$ (D)	peak position (nm)	bandwidth (nm)
$MAPbI_3$	0 ± 0.5	2.4 ± 0.3	760 ± 10	32 ± 2
$MAPbI_2Br$	−1.9 ± 0.8	1.5 ± 0.5	680 ± 16	23 ± 4
$MAPbIBr_2$	−2.2 ± 0.5	3.0 ± 0.3	600 ± 13	23 ± 3
$MAPbBr_3$	−4.1 ± 0.7	2.2 ± 0.5	530 ± 16	14 ± 3

SI (Figures S5–S7). Note that the exciton bands were simulated by assuming a Gaussian band shape. The peak position and bandwidth of the exciton band as well as the magnitude of $\Delta\mu$ ($\equiv|\Delta\boldsymbol{\mu}|$) and $\Delta\bar{\alpha}$ determined with the integral method are shown in Table 1. As shown in Table 1 and Figure 6, the magnitude of $\Delta\mu$ is roughly the same in these

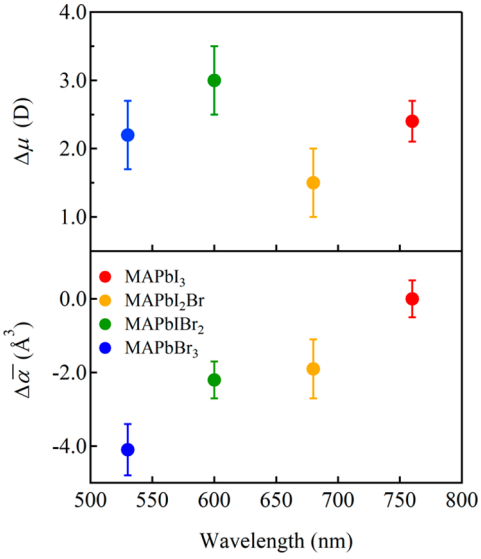

Figure 6. Plots of the magnitudes of $\Delta\boldsymbol{\mu}$ and $\Delta\bar{\alpha}$ following absorption into the first exciton band of $MAPbI_3$, $MAPbI_2Br$, $MAPbIBr_2$, and $MAPbBr_3$.

compounds, while the magnitude of $\Delta\bar{\alpha}$ increases, as the bromine component increases in mixed halides. A comparison of E-A spectra among $MAPbI_{3-x}Br_x$ could not be done with the same grain size. Further, the grain size of the nanocrystal in each sample is not homogeneous, as shown in the SEM images (Figure 1). As will be mentioned in the experimental section, a large size of $MAPbI_3$ crystals having the average size of more than 0.5 μm were prepared by the solvent-annealing method, and it was confirmed that E-A spectra were essentially the same within the experimental error as the ones of the small size crystals having the average diameter of 0.1 μm (shown in Figure 1), indicating that E-A spectra of $MAPbI_3$ are nearly independent of the crystal size. As shown in Figure 1, the average diameter of nanocrystals is in the order of $MAPbBr_2I$ > $MAPbBr_3$ > $MAPbBrI_2$ > $MAPbI_3$, but the magnitude of $\Delta\mu$ and $\Delta\bar{\alpha}$ does not follow the order. Thus, the magnitude of $\Delta\mu$ or $\Delta\bar{\alpha}$ among $MAPbI_{3-x}Br_x$, with $x = 0-3$ has no direct relation with the grain size (cf. Figures 1 and 6), suggesting that the

DOI: 10.1021/acsphotonics.8b00185
ACS Photonics 2018, 5, 2408–2417

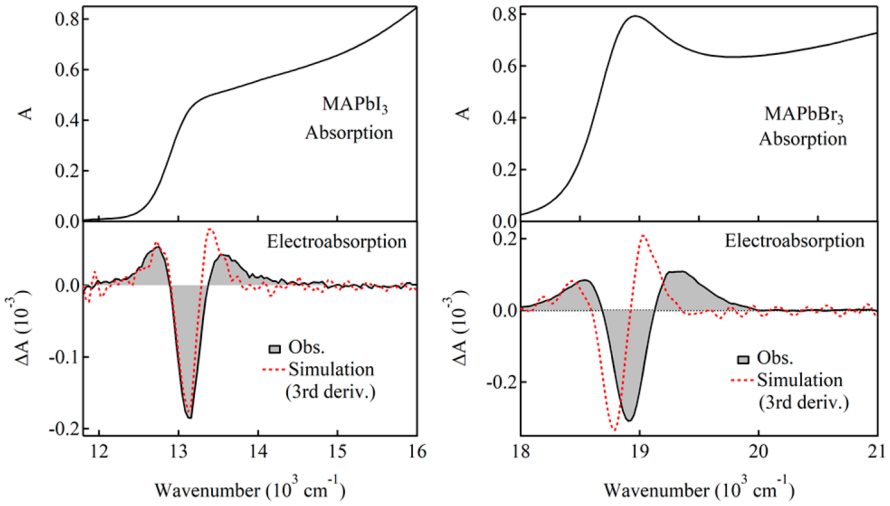

Figure 7. Absorption spectrum (upper) and E-A spectrum (lower) of $MAPbI_3$ (left) and $MAPbBr_3$ (right). The red dotted line shows the third derivative of the absorption spectrum in arbitrary unit.

charge-separated character of the exciton state has no direct relation with the grain size in these materials.

The shape of the E-A spectra as well as the magnitude of $\Delta\mu$ of $MAPbI_3$ reported by Wu et al.[28] is very different from the one obtained in the present study. The present E-A spectra were obtained from the transmitted light intensity of the excitation light, while the E-A spectra reported by Wu et al.[28] were obtained from the reflected light intensity of excitation light. The differences between the line shape measured in our EA spectra of $MAPbI_3$ and those shown in other reports can be explained primarily on the basis of optical effects due to differences in measurement geometry and sample thickness.[28,36,37] The other literature's reports of E-A spectra on $MAPbI_3$ conducted the measurement on relatively thicker films (~200−400 nm) in a reflection geometry, where the sample was oriented at 45° incidence, and the modulation of the reflected signal relative to the total reflective light intensity, $\Delta R/R$, was recorded. In those experiments, the probe light was reflected from a thick (~100 nm) metal back electrode after making its first pass through the film, and then detected after second pass transmission back through the film to the air/glass interface. When E-A spectra are measured in this geometry, $\Delta R/R$ signal may be significantly distorted, in contrast with the $\Delta I_{EX}/I_{EX}$ signal that would be measured in a single pass transmittance geometry, where a semitransparent top electrode is used.[36] The distortion is entirely due to the effects from refractive index modulation, which can be expected for thicker films measured in reflection geometry and optical interference effects.

Ziffer et al.[36] observed E-A spectra of $MAPbI_3$ by monitoring the transmitting light, as in the present experimental procedures. Their E-A spectra of $MAPbI_3$ are very similar to the ones observed in the present experiments. In contrast with the present analysis as well as the analysis done by Wu et al.,[28] where E-A spectra are analyzed by a linear combination of the sum of zeroth, first, and second derivative line shapes, Ziffer et al.[36] hypothesized that the E-A response was related to the Franz-Keldysh-Aspnes (FKA) effect,[38,39] as has been observed in other bulk semiconductors which have binding energy of hole and electron less than 10 meV. The main reason for such hypothesis results from the fact that the observed E-A spectra could not be fitted with the analysis by a combination of zeroth, first, and second derivatives of the observed total absorption spectra. Here, we do not employ their hypothesis because it is considered that the E-A spectra could be analyzed by a combination of the zeroth, first, and second derivatives of the absorption spectra by assuming that absorption spectrum is a superposition of exciton band and continuum band, which result from the absorption of a hole−electron pair and the transition from the valence state to the conduction state, respectively, and that only the exciton absorption band shows strong E-A signal, as already mentioned above.

If FKA effect exists as a contribution from continuum part of the transition, the so-called Franz-Keldysh oscillation should be observed as a result of the band structure of the conduction band modified by electric field. Actually, the Franz-Keldysh oscillation was not identified in the present experiments. According to our preliminary experiments of the temperature dependence of the E-A spectra, the oscillation could not be observed even at low temperatures less than 100 K. The contribution of the continuum band could be neglected in the present analysis of the observed E-A spectra. For the assignment of the E-A spectra of $MAPbI_3$ crystal as the FKA effect, it was stressed that the observed E-A spectra of $MAPbI_3$ could be simulated by the third derivative of the absorption spectra.[36] If it is true, it may be considered that the E-A spectra of other $MAPbI_{3-x}Br_x$ than $MAPbI_3$ should be also fitted by the third derivative of the absorption spectra because all the samples of $MAPbI_{3-x}Br_x$ give similar E-A spectra, as shown in Figure 2. As shown in Figure 7, however, the E-A spectrum of $MAPbBr_3$ cannot be fitted by the third derivative of the total absorption spectrum, though the E-A spectrum of $MAPbI_3$ is similar in shape to the third derivative of the total absorption spectrum. Then, it is considered that the observed E-A spectra of $MAPbI_{3-x}Br_x$ should be analyzed as the Stark shift of the exciton absorption band, that is, as a linear combination of the zeroth, first and second derivatives of the exciton absorption band, as already mentioned. It is noted that the E-A spectra observed for 2D organic−inorganic hybrid perovskite multiple quantum wells ($(C_4H_9NH_3)_2PbI_4$) were explained in terms of FKA effect.[40] The binding energy of this semiconductor was reported to be 190 meV by the same authors and 320 meV by other authors.[41] However, it should be also noted that E-A spectra of 2D exciton in $(C_6H_{13}NH_3)_2PbI_4$ observed at 5 K was

DOI: 10.1021/acsphotonics.8b00185
ACS Photonics 2018, 5, 2408−2417

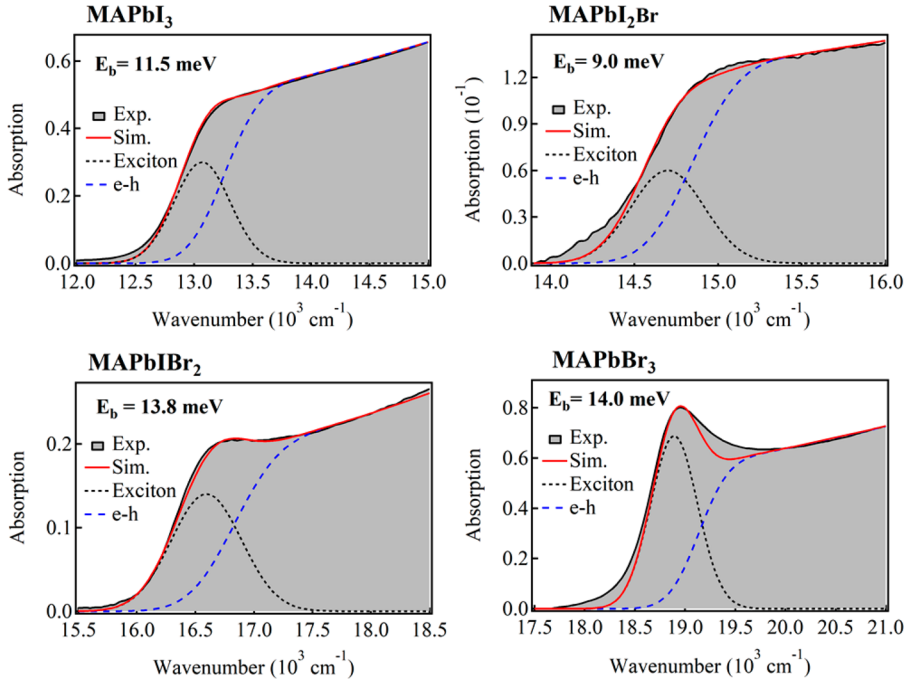

Figure 8. Absorption spectra of mixed halide perovskites $MAPbI_{3-x}Br_x$ (x = 0, 1, 2, and 3) thin films. Shaded line shows the observed spectra, and red line shows the simulated absorption spectrum given by a sum of the exciton band (black dotted line) and continuum band which were simulated with eq 5. The used parameters are shown in Table 2.

explained in terms of the Stark shift,[42] not by the FKA effect. Then, further study may be necessary to fix the origin of the E-A signal in the 2D lead halide samples.

The theoretical work of the effect of applied electric fields on the exciton absorption band suggests that the presence of electric fields results in the shift and broadening of the exciton band.[43,44] The magnitude of the field-induced broadening of the exciton absorption band profile is estimated to be roughly 10 cm^{-1} with a field strength of 0.3 $MVcm^{-1}$, based on the magnitude of $\Delta\mu$ in the present perovskite compounds (roughly 2D, as shown in Table 1). Nonzero value of $\Delta\bar{\alpha}$ except for $MAPbI_3$ also shows a field-induced blue shift of the first exciton band. The magnitude of the shift becomes larger with increasing the bromine component, and $MAPbBr_3$ shows the maximum blue shift by about 0.01 cm^{-1} with a field strength of 0.3 $MV{\cdot}cm^{-1}$.

Simulation of Binding Energy of Exciton. As already mentioned, absorption spectra of $MAPbI_{3-x}Br_x$ (x = 0, 1, 2, and 3) can be separated into the exciton absorption band and the remaining continuum band assigned to the band-to-band transition (see Figures 5 and S5−S7). As shown in SI, the absorption intensity at angular frequency ω can be expressed as follows:

$$A(\omega) = A_{ex}\sum_{n}\frac{\sqrt{E_b}}{n^3}G1(\omega) + A_{e-h}\sum_{k=0}^{Z_{end}/h}G2(\omega) \times \frac{2\pi\sqrt{E_b}}{1-e^{-2\pi(\sqrt{2\beta}\sqrt{E_b}/\sqrt{1-\sqrt{1-4\beta(Z_k-E_g)}})}} \frac{1}{\sqrt{1-4\beta(Z_k-E_g)}} \quad (5)$$

where

$$G1(\omega) = e^{-((\hbar\omega-(E_g-(E_b/n^2)))^2/2\sigma^2)}$$

$$G2(\omega) = e^{-((\hbar\omega-Z_k))^2/2\sigma^2)}$$

Here, the first and second terms in eq 5 correspond to the exciton band and the continuum band, respectively, and Z_k is the k-th dummy variable which has equal space in energy ~0.81 cm^{-1}, β represents the magnitude of non parabolicity of band dispersion, E_b is the binding energy of hole and electron, E_g is the bandgap energy, and the relation of $E_g = \hbar\nu_0 + E_b$ is hold for the exciton band. We use the Gaussian function, G1 and G2, as the line shape function, because the Gaussian shape has been assumed to derive the absorption spectrum of the first exciton band from the E-A spectra using the integral method. σ in eq 5 was estimated from the full-width at the half-maximum (fwhm) of the exciton band. To simulate the observed absorption spectrum as a combination of exciton band and continuum band, fwhm and the center of the exciton band, ν_0, which were obtained from the E-A spectra by the integral method were used (see Table 1). In the simulation, E_b, β, A_{ex}, and $A_{e\text{-}h}$ were changed, and the total absorption spectrum could be reproduced quite well with eq 5 with suitable values of these parameters, as shown in Figure 8. Then, the binding energy of electron and hole, that is, E_b has been determined for each of $MAPbI_{3-x}Br_x$, based on these simulations. The results, that is, fwhm and peak position ($h\nu_0$) of the exciton band, $A_{ex}/A_{e\text{-}h}$, β, and E_b are shown in Table 2. The simulated value of E_b is ranged from 9 to 15 meV in these materials, indicating that the binding energy of these materials is not so different from each other. To show the reliability of the evaluated value of the binding energy, a comparison is made with different binding energy by ±5 meV, with $A_{ex}/A_{e\text{-}h}$ and magnitude of nonparabolicity of band dispersion (β) which are the same as the ones shown in Table 1. The results are shown in SI (Figure S8). Simulation was also done not only with different binding

DOI: 10.1021/acsphotonics.8b00185
ACS Photonics 2018, 5, 2408−2417

Table 2. Fitted Parameters Used for the Theoretical Simulation of Optical Transitions of Uniform-Structured Perovskite under Different Perovskite Thin Films

sample	fwhm (cm^{-1})	$h\nu_0$ (cm^{-1})	$A_{ex}/A_{e\text{-}h}$	β (eV^{-1})	E_b (meV)
$MAPbI_3$	587 ± 40	13068	0.59	0.25	11.5
$MAPbI_2Br$	512 ± 40	14699	0.48	0.10	9.0
$MAPbIBr_2$	708 ± 50	16595	0.74	0.40	13.8
$MAPbBr_3$	510 ± 70	18901	1.18	0.20	14.0

energy but also with different value of $A_{ex}/A_{e\text{-}h}$. One such example is also shown in SI (Figure S9 and Table S1).

It was reported that the photoenergy conversion efficiency in photovoltaic cells constructed with these perovskite compounds is very different from each other.[23] We have reconfirmed these results, as shown in SI (Figure S10). The present results of similar binding energy as well as similar value of $\Delta\mu$ (see Figure 6) imply that the remarkable difference of the photoenergy conversion efficiency in these materials does not come from the difference in concentration of free carriers produced by photoirradiation, but probably comes from the difference in carrier mobility, in addition to the difference in light harvesting efficiency. Regarding the carrier mobility from one nanocrystal to another or carrier injection from nanocrystal to electrode, morphology may play a significant role. By controlling morphology, therefore, carrier mobility as well as efficiency of photoenergy conversion may be increased. It is also noted that the absorption intensity extends to the red, as the iodine component becomes larger in the mixed halide compounds. Information about the carrier dynamics following photoexcitation in the presence of electric field may be obtained from electrophotoluminescecne (E-PL) study, that is, from the electric field effects on photoluminescence.[45]

The ion migration mobility in the presence of electric field was estimated to be 1.5×10^{-9} cm^2 V s^{-1} at 1.5 V μm^{-1}.[46] The small size nanocrystals of $MAPbI_3$ has an average size of 0.1 μm (surface area is roughly 1×10^{-10} cm^2). In case of the sample shown in Figure 3, the distance between FTO and silver electrodes was ~660 nm, and so ~20 V was applied to obtain the field strength of 0.3 MV cm^{-1}. With this applied voltage, the mobility is estimated to be $\sim 3 \times 10^{-8}$ cm^2 s^{-1}. In the present experiments, E-A spectra were measured with application of electric field having modulation frequency of 1 kHz, not DC voltage. In such a case, there is a possibility that ion drift occurs with $\sim 3 \times 10^{-11}$ cm^2 per one cycle of applied ac voltage, which is much smaller than the surface area of single nanocrystals, that is, ions may drift back and forth inside a single nanocrystal during application of ac voltage. The quadratic field strength dependence of the E-A signal suggests that this kind behavior does not affect the electric property of exciton as well as local composition.

As demonstrated in the E-A measurements of solution,[47] reorientation of chromophores induced by applied electric field can be detected by measuring the angle dependence of the E-A spectra, that is, the spectral shape of the E-A spectra observed with 90° and 54.7° (magic angle) as the angle of χ in eqs 1−4 are different from each other, when orientation as well as location of chromophores is affected by applied electric field. As shown in SI (Figure S13), E-A spectra were essentially the same with 90° and magic angle for χ, indicating that applied electric field does not affect the local composition as well as molecular alignment.

Dispersion of $\chi^{(3)}$ of Perovskite Films. Refractive index is changed by application of external electric field. Complex refractive index ($\bar{n}$) can be represented as a sum of the real part (refractive index, n) and imaginary part (extinction coefficient, k) as follows:

$$\bar{n} = n + ik \tag{6}$$

The field-induced change in absorption spectra can be related to the change in reflective index by the following Kramers−Kronig relation:[48,49]

$$n(\nu) - 1 = \frac{1}{2\pi^2} p \int \frac{\beta(\nu)}{\nu'^2 - \nu^2} d\nu'$$
$$\Delta n(\nu) = \frac{1}{2\pi^2} p \int \frac{\Delta\beta(\nu)}{\nu'^2 - \nu^2} d\nu' \tag{7}$$

$$k(\nu) = \frac{\lambda}{4\pi}\beta(\nu)$$
$$\Delta k(\nu) = \frac{\lambda}{4\pi}\Delta\beta(\nu) \tag{8}$$

Here, p represents the principal value of the integral, λ is the wavelength, and $\beta(\nu)$ and $\Delta\beta(\nu)$ are absorption coefficient and its field-induced change, which can be related to absorbance (A) and its field-induced change (ΔA), respectively, as follows: $\beta(\nu) = \ln 10 A(\nu)/L$ and $\Delta\beta(\nu) = \ln 10 A\Delta(\nu)/L$, where L represents thickness of samples.

With these optical quantities, the frequency-dependent third-order nonlinear susceptibility $\chi^{(3)}(-\nu; \nu, 0, 0)$ can be calculated from the following equation:[50]

$$\chi^{(3)}(-\nu; \nu, 0, 0) = \frac{(n\Delta n - k\Delta k)}{6\pi F^2} + i\frac{(n\Delta k + k\Delta n)}{6\pi F^2} \tag{9}$$

Here, F is the external electric field. By using the above equation, the dispersion curve of $\chi^{(3)}(-\nu; \nu, 0, 0)$ was obtained for each of the perovskite samples. As already mentioned, the E-A signal was observed only for the first exciton band, whose absorption spectrum was extracted by the integral method analysis of the E-A spectra. Therefore, the calculation was done in the wavelength region from 400 to 830 nm, by assuming that $\Delta\beta = 0$, that is, $\Delta n = 0$, as well as $\Delta k = 0$, except for the exciton absorption region. The results of the simulation are shown in Figure 9. The value is in the range of $(6-15) \times 10^{-12}$ e.s.u. (electrostatic unit), as shown in Figure 9.

For evaluation of the nonlinear optical property, it is more practical to compare $|\chi^{(3)}(-\nu; \nu, 0, 0)|/\alpha(\nu)$ since the absorption of light is taken into account. Here $\alpha(\nu)$ is the absorption coefficient and given by $A/(\log eL)$, where A and L are the absorbance and thickness of the material, respectively. The absorbance at the peak of the first exciton band is estimated to be 0.30, 0.12, 0.16, and 0.69 for $MAPbI_3$, $MAPbI_2Br$, $MAPbIBr_2$, and $MAPbBr_3$, respectively (see Figures 5 and S5−S7), while the thickness of the perovskite solid films corresponding to these samples is 270, 62.5, 66.8, and 198 nm, respectively. Then, $|\chi^{(3)}(-\nu; \nu, 0, 0)|/\alpha(\nu)$ is determined to be 4.4×10^{-16}, 5.9×10^{-16}, 2.3×10^{-16}, and 1.0×10^{-16} e.s.u. cm for $MAPbI_3$, $MAPbI_2Br$, $MAPbIBr_2$, and $MAPbBr_3$, respectively, showing a trend of the decrease of the third-order nonlinear susceptibility with increasing bromine component. These values are much smaller than those for conjugated polymers, $(5 \pm 3) \times 10^{-14}$ e.s.u. cm. Thus, the nonlinear optical

DOI: 10.1021/acsphotonics.8b00185
ACS Photonics 2018, 5, 2408−2417

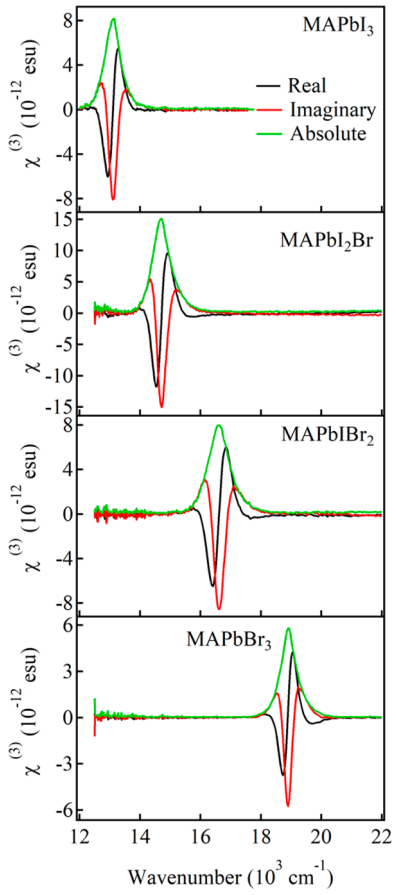

Figure 9. Real part (black line) and the imaginary part (red line) of $\chi^{(3)}$ obtained using the E-A spectra of $MAPbI_3$, $MAPbI_2Br$, $MAPbIBr_2$, and $MAPbBr_3$. Absolute value is also shown in the figure (green).

parameter of perovskites is rather small, indicating the field-induced change in refractive index is rather small in the present perovskites. In π-conjugated polymers, the third-order nonlinear optical property is very sensitive to the length of the π-electron conjugation. The fact that the magnitude of $\chi^{(3)}$ of the present nanocrystals of $MAPbI_{3-x}Br_x$ is much smaller than those in π-conjugated polymers may indicate that electrons in these perovskites are localized in the small region of the network of metal halide PbX_6 (X = Br and I) octahedral with organic cation spacer MA.

CONCLUSIONS

Electroabsorption (E-A) spectra of nanocrystalline films of methylammonium lead halide prerovskites, $MAPbI_{3-x}Br_x$ (x = 0, 1, 2, and 3) have been obtained by measuring the transmitted light intensity of the excitation light. The E-A spectra have been analyzed by assuming that the E-A signal is caused by the Stark shift, whose signal is given by a linear combination of the zeroth, first and second derivatives of the exciton absorption band in every material, and it is considered that the E-A signal of the continuum band is negligibly small. By using the integral method analysis for the E-A spectra, the magnitudes of the change in electric dipole moment ($\Delta\mu$) and in electric polarizability ($\Delta\bar{\alpha}$) between the ground state and the exciton state as well as the clear shape of the exciton absorption band have been determined. The magnitude of $\Delta\mu$ for the exciton band is nearly the same in these materials, while the magnitude of $\Delta\alpha$ slightly increases with increasing the bromine component. Based on the spectral shape as well as the position of the exciton band determined by the integral method analysis of the E-A spectra, the total absorption spectra could be reconstructed, and binding energy of hole−electron pair at the exciton state could be evaluated. In photovoltaic cells constructed with $MAPbI_{3-x}Br_x$, the photoenergy conversion efficiency drastically decreases with increasing the bromide component. The fact that the magnitude of $\Delta\mu$ as well as the binding energy is nearly the same in these materials implies that the drastic difference in photoenergy conversion results from the drastic difference of mobility of free carriers produced by photoirradiation and from the difference of the light harvesting effect, not from the difference in efficiency of photoinduced free carrier generation. Information about the carrier dynamics following photoexcitation in the presence of electric field may be obtained from E-PL study, that is, from the electric field effects on photoluminescence, which will be a future problem. The frequency-dependent third-order nonlinear susceptibility could be also obtained from the E-A spectra in these materials by using the Kramers−Kronig relation. In the results, the nonlinear optical parameter of the perovskites is rather small, and clear relation between the nonlinear optical property and the crystal size or morphology could not be found in the present perovskites.

MATERIALS AND METHODS

Sample Preparation. $MAPbI_3$ was prepared as follows: PbI_2 (Aldrich, 96%, 574 mg) and CH_3NH_3I (homemade, 198 mg) powders were mixed in 1 mL of DMF, which was stirred for 12 h and homogeneous solution was achieved; then, suitable amount of solution (0.3 mL) was dropped on FTO-coated substrate, and spin-coating was done with 5000 rpm for 30 s. We used chlorobenzene (0.2 mL) as antisolvent and dropped it directly on the center of the substrate during the spin coating procedure. After annealing at 100 °C for 10 min, the reaction completed, and the color changed from transparent to black. Then, the small-sized perovskite film which was shown in Figure 1 was obtained. For large sized nanocrystals, the so-called solvent-annealing was used; as the post-treatment, the small-sized perovskite film was put into a Petri dish with 10 mL of DMF and kept at 100 °C for 10 min.

$MAPbI_2Br$ was prepared as follows: PbI_2 (Aldrich, 96%, 574 mg) and CH_3NH_3Br (homemade, 139.4 mg) powders were mixed in 1 mL of 1-methyl-2 pyrrolidinone, which was stirred for 12 h, and homogeneous solution was obtained; then, suitable amount of solution (0.3 mL) was dropped on substrate and spin-coating was done with 4000 rpm for 30 s. After it was immersed in ether for 2 min, the reaction completed, and the color changed from transparent to light brown.

$MAPbIBr_2$ was prepared as follows: $PbBr_2$ (Alfa, 99%, 457 mg) and CH_3NH_3I (homemade, 198 mg) powders were mixed in 1 mL of 1-methyl-2 pyrrolidinone and stirred for 12 h to achieve homogeneous solution; then, a suitable amount of solution (0.3 mL) was dropped on substrate, and spin-coating was done with 4000 rpm for 30 s. After it was immersed in ether for 2 min, the reaction was completed, and the color changed from transparent to orange.

$MAPbBr_3$ was prepared as follows: $PbBr_2$ (Alfa, 99%, 457 mg) and CH_3NH_3Br (homemade, 139.4 mg) powders were mixed in 1 mL of 1-methyl-2 pyrrolidinone and stirred for 12 h to achieve homogeneous solution; then, suitable amount of solution (0.3 mL) was dropped on substrate and spin-coating was done with 4000 rpm for 30 s. After it was immersed in

DOI: 10.1021/acsphotonics.8b00185
ACS Photonics 2018, 5, 2408−2417

ether for 2 min, the reaction completed, and the color changed from transparent to yellow. The SEM images of $MAPbI_3$, $MAPbI_2Br$, $MAPbIBr_2$, and $MAPbBr_3$ thus prepared are shown in Figure 1.

All of the perovskite samples used for the E-A measurements were fabricated by a spin coating method. Before the preparation of perovskite nanocrystalline film on FTO substrates, the substrates were immersed in isopropanol, acetone and deionized water in turn and then cleaned by ultrasonic oscillator for 20 min. After that, it was dried by N_2 and treated with UV ozone for 10 min prior to spin coating.

By dissolving 0.4 g PMMA into 10 mL benzene, PMMA film was spin coated as an insulator on FTO-coated substrate having a perovskite layer. The PMMA layer also prevents perovskite from decomposition. The sample substrates having PMMA film on perovskite sample layer were transferred to a vacuum system (10^{-6} Torr), and silver film was deposited on the PMMA film with a thickness of 25 nm by thermal evaporation. Silver film and FTO film were used as electrodes in the E-A measurements. Thickness of perovskite layers were determined by SEM measurements, and the total thickness of perovskite and PMMA layers were determined by using SEM and profilometer (Dektak 150).

Electroabsorption Measurements. All the measurements were performed at room temperature. Electric field modulation spectroscopy was applied to measure E-A spectra, with the commercially available apparatus (EMV 100, JASCO).[47] A modulation in transmitted light intensity of the excitation light (I_{EX}) was induced by application of the sinusoidal ac voltage with a modulation frequency of 1 kHz. Field-induced change in transmitted light intensity (ΔI_{EX}) was detected with a lock-in amplifier at the second harmonic of the modulation frequency. The dc component of I_{EX} was simultaneously observed. Note that the field-induced change in absorbance (ΔA) is given by $(\Delta I_{EX}/I_{EX})\log e$, when $\Delta I_{EX} \ll I_{EX}$. E-A spectra were obtained by plotting ΔA, as a function of wavelength or wavenumber. The angle between the direction of the applied electric field and the electric vector of the excitation light (χ) was usually set to 90° in the E-A measurements. As occasion demands, magic angle (54.7°) was used for χ.

■ ASSOCIATED CONTENT

Supporting Information

The Supporting Information is available free of charge on the ACS Publications website at DOI: 10.1021/acsphotonics.8b00185.

Sample preparation, field strength dependence of E-A spectra, XRD spectra, integral method analysis of E-A spectra, simulation of binding energy, $I-V$ curves and IPCE curves, formula of optical absorption for exciton and band-to-band transition, polarization dependence of the E-A spectra, and references (PDF).

■ AUTHOR INFORMATION

Corresponding Authors

*E-mail: diau@mail.nctu.edu.tw. Tel.: +886 3 5131524.
*E-mail: nohta@nctu.edu.tw. Tel.: +886 3 5131395.

ORCID

Eric Wei-Guang Diau: 0000-0001-6113-5679
Nobuhiro Ohta: 0000-0003-4255-6448

Notes

The authors declare no competing financial interest.

■ ACKNOWLEDGMENTS

Center for Interdisciplinary Science of NCTU and the Ministry of Science and Technology of Taiwan (MOST 105-2113-M-009-003; MOST 106-2113-M-009-002; MOST 105-2119-M-009-011-MY3) provided financial support of this research. This work was also supported by MOST (MOST 107-3017-F009-003) and by the Center for Emergent Functional Matter Science of National Chiao Tung University from the Featured Areas Research Center Program within the framework of the Higher Education Sprout Project by the Ministry of Education (MOE) in Taiwan.

■ REFERENCES

(1) Wu, M. K.; Ashburn, J. R.; Torng, C. J.; Hor, P. H.; Meng, R. L.; Gao, L.; Huang, Z. J.; Wang, Y. Q.; Chu, C. W. Superconductivity at 93 K in a New Mixed-Phase Y-Ba-Cu-O Compound System at Ambient Pressure. *Phys. Rev. Lett.* **1987**, *58*, 908−910.

(2) Bednorz, J. G.; Müller, K. A. Perovskite-Type Oxides—the New Approach to High-T_C Superconductivity. *Rev. Mod. Phys.* **1988**, *60*, 585−600.

(3) Mitzi, D. B.; Feild, C. A.; Harrison, W. T. A.; Guloy, A. M. Conducting Tin Halides with a Layered Organic-Based Perovskite Structure. *Nature* **1994**, *369*, 467−469.

(4) Smyth, D. M. Perovskite: the Electrically Active Structure. *Ferroelectrics* **2009**, *380*, 1−13.

(5) Fan, Z.; Xiao, J.; Sun, K.; Chen, L.; Hu, Y.; Ouyang, J.; Ong, K. P.; Zeng, K.; Wang, J. Ferroelectricity of $CH_3NH_3PbI_3$ Perovskite. *J. Phys. Chem. Lett.* **2015**, *6*, 1155−1161.

(6) Mitzi, D. B.; Wang, S.; Feild, C. A.; Chess, C. A.; Guloy, A. M. Conducting Layered Organic-Inorganic Halides Containing < 110>-Oriented Perovskite Sheets. *Science* **1995**, *267*, 1473−1476.

(7) Kojima, A.; Teshima, K.; Shirai, Y.; Miyasaka, T. Organometal Halide Perovskites as Visible-Light Sensitizers for Photovoltaic Cells. *J. Am. Chem. Soc.* **2009**, *131*, 6050−6051.

(8) Kim, H.-S.; Lee, C.-R.; Im, J.-H.; Lee, K.-B.; Moehl, T.; Marchioro, A.; Moon, S.-J.; Humphry-Baker, R.; Yum, J.-H.; Moser, J.-E.; et al. Lead Iodide Perovskite Sensitized All-Solid-State Submicron Thin Film Mesoscopic Solar Cell with Efficiency Exceeding 9%. *Sci. Rep.* **2012**, *2*, 591.

(9) Lee, M. M.; Teuscher, J.; Miyasaka, T.; Murakami, T. N.; Snaith, H. J. Efficient Hybrid Solar Cells Based on Meso-Superstructured Organometal Halide Perovskites. *Science* **2012**, *338*, 643−647.

(10) Burschka, J.; Pellet, N.; Moon, S.-J.; Humphry-Baker, R.; Gao, P.; Nazeeruddin, M. K.; Grätzel, M. Sequential Deposition as a Route to High-Performance Perovskite-Sensitized Solar Cells. *Nature* **2013**, *499*, 316−320.

(11) Park, N.-G. Perovskite Solar Cells: an Emerging Photovoltaic Technology. *Mater. Today* **2015**, *18*, 65−72.

(12) Stranks, S. D.; Snaith, H. J. Metal-Halide Perovskites for Photovoltaic and Light-Emitting Devices. *Nat. Nanotechnol.* **2015**, *10*, 391−402.

(13) Descher, F.; Price, M.; Pathak, S.; Klintberg, L. E.; Jarausch, D. D.; Higler, R.; Huttner, S.; Leijtens, T.; Stranks, S. D.; Snaith, H. J.; Atature, M.; Phillips, R. T.; Friend, R. H. Photoluminescence Efficiency and Optically Pumped Lasing in Solution-Processed Mixed Halide Perovskite Semiconductors. *J. Phys. Chem. Lett.* **2014**, *5*, 1421−1426.

(14) Sheng, C.; Zhang, C.; Zhai, Y.; Mielczarek, K.; Wang, W.; Ma, W.; Zakhidov, A.; Vardeny, Z. V. Exciton Versus Free Carrier Photogeneration in Organometal Trihalide Perovskites Probed by Broadband Ultrafast Polarization Memory Dynamics. *Phys. Rev. Lett.* **2015**, *114*, 116601.

(15) Savenije, T. J.; Ponseca, C. S.; Kunneman, L.; Abdellah, M.; Zheng, K.; Tian, Y.; Zhu, Q.; Canton, S. E.; Scheblykin, I. G.; Pullerits, T.; Yartsev, A.; Sundström, V. Thermally Activated Exciton Dissociation and Recombination Control the Carrier Dynamics in

DOI: 10.1021/acsphotonics.8b00185
ACS Photonics 2018, 5, 2408−2417

Organometal Halide Perovskite. *J. Phys. Chem. Lett.* **2014**, *5*, 2189−2194.
(16) Manser, J. S.; Christians, J. A.; Kamat, P. V. Intriguing Optoelectronic Properties of Metal Halide Perovskites. *Chem. Rev.* **2016**, *116*, 12956−13008.
(17) Stoumpos, C. C.; Kanatzidis, M. G. The Renaissance of Halide Perovskites and Their Evolution as Emerging Semiconductors. *Acc. Chem. Res.* **2015**, *48*, 2791−2802.
(18) Christians, J. A.; Manser, J. S.; Kamat, P. V. Multifaceted Excited State of $CH_3NH_3PbI_3$. Charge Separation, Recombination, and Trapping. *J. Phys. Chem. Lett.* **2015**, *6* (11), 2086−2095.
(19) Dong, Q.; Fang, Y.; Shao, Y.; Mulligan, P.; Qiu, J.; Cao, L.; Huang, J. Electron-Hole Diffusion Lengths > 175 μm in Solution-Grown $CH_3NH_3PbI_3$ Single Crystals. *Science* **2015**, *347*, 967−970.
(20) Shi, D.; Adinolfi, V.; Comin, R.; Yuan, M.; Alarousu, E.; Buin, A.; Chen, Y.; Hoogland, S.; Rothenberger, A.; Katsiev, K.; et al. Low Trap-State Density and Long Carrier Diffusion in Organolead Trihalide Perovskite Single Crystals. *Science* **2015**, *347*, 519−522.
(21) Ohta, N.; Awasthi, K.; Okoshi, K.; Manseki, K.; Miura, H.; Inoue, Y.; Nakamura, K.; Kono, H.; Diau, E. W.-G. Stark Spectroscopy of Absorption and Emission of Indoline Sensitizers: a Correlation with the Performance of Photovoltaic Cells. *J. Phys. Chem. C* **2016**, *120*, 26206−26216.
(22) Awasthi, K.; Hsu, H.-Y.; Diau, E. W.-G.; Ohta, N. Enhanced Charge Transfer Character of Photoexcited States of Dye Sensitizer on the N719/TiO_2 Interface as Revealed by Electroabsorption Spectra. *J. Photochem. Photobiol., A* **2014**, *288*, 70−75.
(23) Cui, D.; Yang, Z.; Yang, D.; Ren, X.; Liu, Y.; Wei, Q.; Fan, H.; Zeng, J.; Liu, S. F. Color-Tuned Perovskite Films Prepared for Efficient Solar Cell Applications. *J. Phys. Chem. C* **2016**, *120*, 42−47.
(24) Noh, J. H.; Im, S. H.; Heo, J. H.; Mandal, T. N.; Seok, S. I. Chemical Management for Colorful, Efficient, and Stable Inorganic−Organic Hybrid Nanostructured Solar Cells. *Nano Lett.* **2013**, *13*, 1764−1769.
(25) Gil-Escrig, L.; Miquel-Sempere, A.; Sessolo, M.; Bolink, H. J. Mixed Iodide−Bromide Methylammonium Lead Perovskite-Based Diodes for Light Emission and Photovoltaics. *J. Phys. Chem. Lett.* **2015**, *6*, 3743−3748.
(26) Tu, Y.; Wu, J.; Lan, Z.; He, X.; Dong, J.; Jia, J.; Guo, P.; Lin, J.; Huang, M.; Huang, Y. Modulated $CH_3NH_3PbI_{3-X}Br_X$ Film for Efficient Perovskite Solar Cells Exceeding 18%. *Sci. Rep.* **2017**, *7*, 44603.
(27) Yuan, D.-X.; Yuan, X.-D.; Xu, Q.-Y.; Xu, M.-F.; Shi, X. B.; Wang, Z. K.; Liao, L. S. A Solution-Processed Bathocuproine Cathode Interfacial Layer for High-Performance Bromine−Iodine Perovskite Solar Cells. *Phys. Chem. Chem. Phys.* **2015**, *17*, 26653−26658.
(28) Wu, X.; Yu, H.; Li, L.; Wang, F.; Xu, H.; Zhao, N. Composition-Dependent Light-Induced Dipole Moment Change in Organometal Halide Perovskites. *J. Phys. Chem. C* **2015**, *119*, 1253−1259.
(29) Liptay, W. Dipole Moments and Polarizabilities of Molecules in Excited Electronic States. *Excited States* **1974**, *1*, 129−229.
(30) Locknar, S. A.; Peteanu, L. A. Investigation of the Relationship Between Dipolar Properties and Cis−Trans Configuration in Retinal Polyenes: a Comparative Study Using Stark Spectroscopy and Semiempirical Calculations. *J. Phys. Chem. B* **1998**, *102*, 4240−4246.
(31) Bublitz, G. U.; Boxer, S. G. Stark Spectroscopy: Applications in Chemistry, Biology and Materials Science. *Annu. Rev. Phys. Chem.* **1997**, *48*, 213−242.
(32) Jalviste, E.; Ohta, N. Theoretical Foundation of Electro-absorption Spectroscopy: Self-Contained Derivation of the Basic Equations with the Direction Cosine Method and the Euler Angle Method. *J. Photochem. Photobiol., C* **2007**, *8*, 30−46.
(33) Awasthi, K.; Iimori, T.; Ohta, N. Integral Method Analysis of Electroabsorption Spectra and Its Application to Quantum Dots of PbSe. *J. Phys. Chem. C* **2014**, *118*, 18170−18176.
(34) Awasthi, K.; Iimori, T.; Ohta, N. Electroabsorption Spectra of Quantum Dots of PbS and Analysis by the Integral Method. *J. Phys. Chem. C* **2015**, *119*, 4351−4361.
(35) Novelli, F.; Fausti, D.; Giusti, F.; Parmigiani, F.; Hoffmann, M. Mixed Regime of Light-Matter Interaction Revealed by Phase Sensitive Measurements of the Dynamical Franz-Keldysh Effect. *Sci. Rep.* **2013**, *3*, 1227.
(36) Ziffer, M. E.; Mohammed, J. C.; Ginger, D. S. Electroabsorption Spectroscopy Measurements of the Exciton Binding Energy, Electron−Hole Reduced Effective Mass, and Band Gap in the Perovskite $CH_3NH_3PbI_3$. *ACS Photonics* **2016**, *3*, 1060−1068.
(37) Roiati, V.; Mosconi, E.; Listorti, A.; Colella, S.; Gigli, G.; De Angelis, F. Stark Effect in Perovskite/TiO_2 Solar Cells: Evidence of Local Interfacial Order. *Nano Lett.* **2014**, *14*, 2168−2174.
(38) Aspnes, D. E. Direct Verification of the Third-Derivative Nature of Electroreflectance Spectra. *Phys. Rev. Lett.* **1972**, *28*, 168−171.
(39) Aspnes, D. E.; Rowe, J. E. Resonant Nonlinear Optical Susceptibility: Electroreflectance in the Low-Field Limit. *Phys. Rev. B* **1972**, *5*, 4022−4030.
(40) Amerling, E.; Baniya, S.; Lafalce, E.; Zhang, C.; Vardeny, Z. V.; Whittaker-Brooks, L. Electroabsorption Spectroscopy Studies of $(C_4H_9NH_3)_2PbI_4$ Organic-Inorganic Hybrid Perovskite Multiple Quantum Wells. *J. Phys. Chem. Lett.* **2017**, *8*, 4557−4564.
(41) Ishihara, T.; Takahashi, J.; Goto, T. Optical Properties Due to Electronic Transitions in Two-Dimensional Semiconductors $(C_nH_{2n+1}NH_3)_2PbI_4$. *Phys. Rev. B: Condens. Matter Mater. Phys.* **1990**, *42*, 11099.
(42) Tanaka, K.; Sano, F.; Takahashi, T.; Kondo, T.; Ito, R.; Ema, K. Two-Dimensional Wannier Excitons in a Layered-Perovskite-Type Crystal $(C_6H_{13}NH_3)_2PbI_4$. *Solid State Commun.* **2002**, *122*, 249−252.
(43) Ralph, H. I. On the Theory of the Franz-Keldysh Effect. *J. Phys. C: Solid State Phys.* **1968**, *1*, 378−386.
(44) Blossey, D. F. Wannier Exciton in an Electric Field. I. Optical Absorption by Bound and Continuum States. *Phys. Rev. B* **1970**, *2*, 3976−3990.
(45) Awasthi, K.; Wang, C.-Y.; Fathi, A.; Narra, S.; Diau, E. W.-G.; G, E. W.; Ohta, N. Anisotropic Electric Field Effect on Photo-luminescence of $CH_3NH_3PbI_3$ Perovskite Sandwiched between Conducting and Insulating Films. *J. Phys. Chem. C* **2017**, *121*, 22700−22706.
(46) Yuan, Y.; Chae, J.; Shao, Y.; Wang, Q.; Xiao, Z.; Centrone, A.; Huang, J. Photovoltaic Switching Mechanism in Lateral Structure Hybrid Perovskite Solar Cells. *Adv. Energy Mater.* **2015**, *5*, 1500615.
(47) Tayama, J.; Iimori, T.; Ohta, N. Comparative Study of Electroabsorption Spectra of Polar and Nonpolar Organic Molecules in Solution and in a Polymer Film. *J. Chem. Phys.* **2009**, *131*, 244509.
(48) Weiner, J. S.; Miller, D. A. B.; Chemla, D. S. Quadratic Electro-Optic Effect Due to the Quantum-Confined Stark Effect in Quantum Wells. *Appl. Phys. Lett.* **1987**, *50*, 842−844.
(49) Phillips, S. D.; Worland, R.; Yu, G.; Hagler, T.; Freedmann, R.; Cao, Y.; Yoon, V.; Chiang, J.; Walker, W. C.; Heeger, A. J. Electroabsorption of Polyacetylene. *Phys. Rev. B: Condens. Matter Mater. Phys.* **1989**, *40*, 9751−9759.
(50) Umeuchi, S.; Nishimura, Y.; Yamazaki, I.; Murakami, H.; Yamashita, M.; Ohta, N. Electric Field Effects on Absorption and Fluorescence Spectra of Pyrene Doped in a PMMA Polymer Film. *Thin Solid Films* **1997**, *311*, 239−245.

DOI: 10.1021/acsphotonics.8b00185
ACS Photonics 2018, 5, 2408−2417